DAXX-dependent supply of soluble (H3.3–H4) dimers to PML bodies pending deposition into chromatin

Erwan Delbarre, Kristina Ivanauskiene, Thomas Küntziger, et al.

Genome Res. 2013 23: 440-451 originally published online December 5, 2012
Access the most recent version at doi:10.1101/gr.142703.112

DAXX-dependent supply of soluble (H3.3–H4) dimers to PML bodies pending deposition into chromatin

Erwan Delbarre,[1,2] Kristina Ivanauskiene,[1,2] Thomas Küntziger,[1,2] and Philippe Collas[1,2,3]

[1]*Stem Cell Epigenetics Laboratory, Institute of Basic Medical Sciences, Faculty of Medicine, University of Oslo, 0317 Oslo, Norway;* [2]*Norwegian Center for Stem Cell Research, University of Oslo, 0317 Oslo, Norway*

Replication-independent chromatin deposition of histone variant H3.3 is mediated by several chaperones. We report a multistep targeting of newly synthesized epitope-tagged H3.3 to chromatin via PML bodies. H3.3 is recruited to PML bodies in a DAXX-dependent manner, a process facilitated by ASFIA. DAXX is required for enrichment of ATRX, but not ASFIA or HIRA, with PML. Nonetheless, the chaperones colocalize with H3.3 at PML bodies and are found in one or more complexes with PML. Both DAXX and PML are necessary to prevent accumulation of a soluble, nonincorporated pool of H3.3. H3.3 targeting to PML is enhanced with an $(H3.3–H4)_2$ tetramerization mutant of H3.3, suggesting H3.3 recruitment to PML as an (H3.3–H4) dimer rather than as a tetramer. Our data support a model of DAXX-mediated recruitment of (H3.3–H4) dimers to PML bodies, which may function as triage centers for H3.3 deposition into chromatin by distinct chaperones.

[Supplemental material is available for this article.]

The duplication of eukaryotic chromosomes during S phase requires DNA replication and a doubling in the number of nucleosomes. This necessitates a pool of available canonical histones, whose production is tightly coupled to DNA replication (Marzluff et al. 2008). Additionally, processes such as DNA repair and transcription require eviction, addition, or replacement of nucleosomes also outside S phase and involve histone variants. Histone variants are paralogs of canonical histones and have been identified for H1, H2A, H2B, and H3; they are expressed throughout the cell cycle and are incorporated into chromatin independently of DNA synthesis (Talbert and Henikoff 2010). Because of their incorporation into distinct chromatin domains, the mechanisms of chromatin deposition of histone variants have in recent years sparked much research interest, in particular for histone H3 which together with H4 constitutes the core of the nucleosome.

In addition to the centromeric variant CENPA, histone H3 has three major isoforms in mammals, namely, H3.1, H3.2 (often referred to as H3), and H3.3 (Ederveen et al. 2011). H3.2 and H3.1 differ by a single amino acid, and H3.3 differs from H3.2 and H3.1 by four and five amino acids, respectively. H3.1 and H3.2 are expressed only during S phase, require DNA synthesis for chromatin deposition, and associate preferentially with marks of heterochromatin (Hake and Allis 2006; Tamura et al. 2009; Delbarre et al. 2010). H3.3 is expressed throughout the cell cycle and is incorporated independently of DNA replication (Ahmad and Henikoff 2002). H3.3 has been shown to accumulate at promoters and gene bodies of transcriptionally active and of some inactive genes (Ahmad and Henikoff 2002; McKittrick et al. 2004; Chow et al. 2005; Mito et al. 2005; Daury et al. 2006; Jin and Felsenfeld 2006; Jin et al. 2009; Sutcliffe et al. 2009; Tamura et al. 2009; Delbarre et al. 2010), and recent studies reveal H3.3 deposition also into telomeric and pericentric regions (Goldberg et al. 2010; Wong et al. 2009). H3.3 is therefore represented in a variety of chromatin states and functional sequence elements.

[3]Corresponding author
E-mail philippe.collas@medisin.uio.no
Article published online before print. Article, supplemental material, and publication date are at http://www.genome.org/cgi/doi/10.1101/gr.142703.112.

The discovery of several histone-specific chaperones has shed light on pathways of chromatin deposition of histone variants, particularly of H3.3. Chromatin assembly factor 1 (CAF1) and histone regulator A (HIRA) were the first H3 chaperones to be identified and suggested to account, at least in part, for the distinct modes of incorporation of H3.1 and H3.3 into chromatin (Tagami et al. 2004). CAF1 binds preferentially to the (H3.1–H4) dimer in cells and enables DNA replication-coupled histone deposition (Smith and Stillman 1989; Tagami et al. 2004). HIRA binds specifically to the (H3.3–H4) dimer and mediates replication-independent incorporation (Ray-Gallet et al. 2002, 2011; Tagami et al. 2004). HIRA belongs to a larger complex composed of at least two other proteins, calcineurin-binding protein 1 (CABIN1) and ubinuclein 1 (UBN1), that are both also involved in H3.3 deposition into chromatin during transcription (Tagami et al. 2004; Balaji et al. 2009; Banumathy et al. 2009; Rai et al. 2011). CAF1 and the HIRA/UBN1/CABIN1 complex can both associate with antisilencing function 1 A (ASF1A), a chaperone able to bind (H3.1–H4) and (H3.3–H4) dimers (Tyler et al. 2001; Mello et al. 2002; Tagami et al. 2004; Zhang et al. 2005; Tang et al. 2006).

More recently, two other interacting histone chaperones, death associated protein (DAXX) and alpha-thalassemia/mental retardation X-linked syndrome protein (ATRX), have been shown to be specific for H3.3 (Drane et al. 2010; Goldberg et al. 2010; Lewis et al. 2010; Wong et al. 2010). Mutations in ATRX and DAXX have been found to be associated with driver H3.3 mutations in pediatric glioblastoma multiform, implicating the H3.3–DAXX–ATRX axis in cancer (Schwartzentruber et al. 2012; Wu et al. 2012). DAXX and ATRX belong to a complex distinct from that formed by HIRA, UBN1, CABIN1, and ASF1A (Drane et al. 2010; Lewis et al. 2010). Moreover, recent structural data from Elsässer and colleagues show that DAXX envelops the (H3.3–H4) dimer in a manner excluding interaction with ASF1 or DNA (Elsasser et al. 2012). DAXX and ATRX deposit (H3.3–H4) into telomeric and pericentric chromatin (Drane et al. 2010; Goldberg et al. 2010; Lewis et al. 2010; Wong et al. 2010), and both are required for chromatin assembly and transcriptional repression of transgene arrays (Newhart et al. 2012). In mouse embryonic cortical neurons, DAXX is involved in H3.3 deposition into regulatory elements of several

23:440–451 © 2013, Published by Cold Spring Harbor Laboratory Press; ISSN 1088-9051/13; www.genome.org

genes activated upon neuronal induction (Michod et al. 2012). Despite recent studies highlighting the role of the ATRX–DNMT3–DNMT3L (ADD) domain of ATRX in H3.3 deposition into heterochromatin (Eustermann et al. 2011; Iwase et al. 2011), the mechanism of H3.3 deposition mediated by DAXX or ATRX remains elusive. Moreover, the existence of at least two molecular complexes targeting H3.3 to different chromatin domains, namely, ASF1A/HIRA/UBN1/CABIN1 and DAXX/ATRX, implies spatial and/or temporal regulation of H3.3 distribution between these complexes. How the pool of newly synthesized and soluble H3.3 is segregated between the chaperone complexes remains undetermined.

Thus far, one study has focused on the deposition of newly synthesized H3.3 into chromatin (Ray-Gallet et al. 2011). This work shows that in HeLa cells, HIRA is the main chaperone involved in the deposition of newly synthesized H3.3 throughout the cell cycle. Down-regulation of HIRA, but not DAXX or ATRX, results in reduced incorporation of an epitope-tagged H3.3, evaluated by measuring the soluble pool of neo-synthesized H3.3. Incorporation of newly synthesized H3.3 can nevertheless occur in other insoluble structures such as promyelocytic leukemia (PML)/Nuclear Domain 10 (ND10) bodies (Drane et al. 2010). These observations suggest a model in which neo-synthesized H3.3 transits through specific intranuclear loci prior to deposition into chromatin; this model, however, has not been tested.

In this study, we use quantitative fluorescence imaging in slow-cycling human primary cells to determine mechanisms addressing newly synthesized epitope-tagged H3.3 to chromatin outside S phase. We demonstrate an H3.3-specific, multistep path of chromatin deposition involving a DAXX-dependent recruitment of soluble (H3.3–H4) dimers to PML bodies, a process facilitated by ASF1A. Together with the enrichment of a fraction of HIRA, ASF1A, DAXX, and ATRX at PML bodies, our results suggest a model of PML bodies as triage centers for soluble H3.3, where it may pair up with distinct chaperones before deposition into chromatin.

Results

Epitope-tagged H3.3 incorporates into chromatin in a multistep manner

The study of H3.3 deposition into chromatin has previously relied on cell lines stably expressing epitope-tagged H3.3. In these cells, exogenous H3.3 is incorporated outside S phase, as well as during S phase together with the replicative variants H3.1 and H3.2. Here, we focus on H3.3 deposition outside S phase, in experiments that minimally perturb the cell cycle. We took advantage of a human primary mesenchymal stem cell type with a long doubling time (~70 h) (Boquest et al. 2005), which we have recently shown incorporates EGFP-tagged H3.3 into chromatin (Delbarre et al. 2010). More than 90% of these cells are in G_1 phase in nonsynchronized cultures (Gaustad et al. 2004), providing a robust opportunity to investigate the pathway of H3.3 deposition into chromatin outside S phase.

Transient transfection of H3.3 tagged with mCherry (H3.3-mC) results in three distinct H3.3 distribution patterns after 24 h (Fig. 1A).

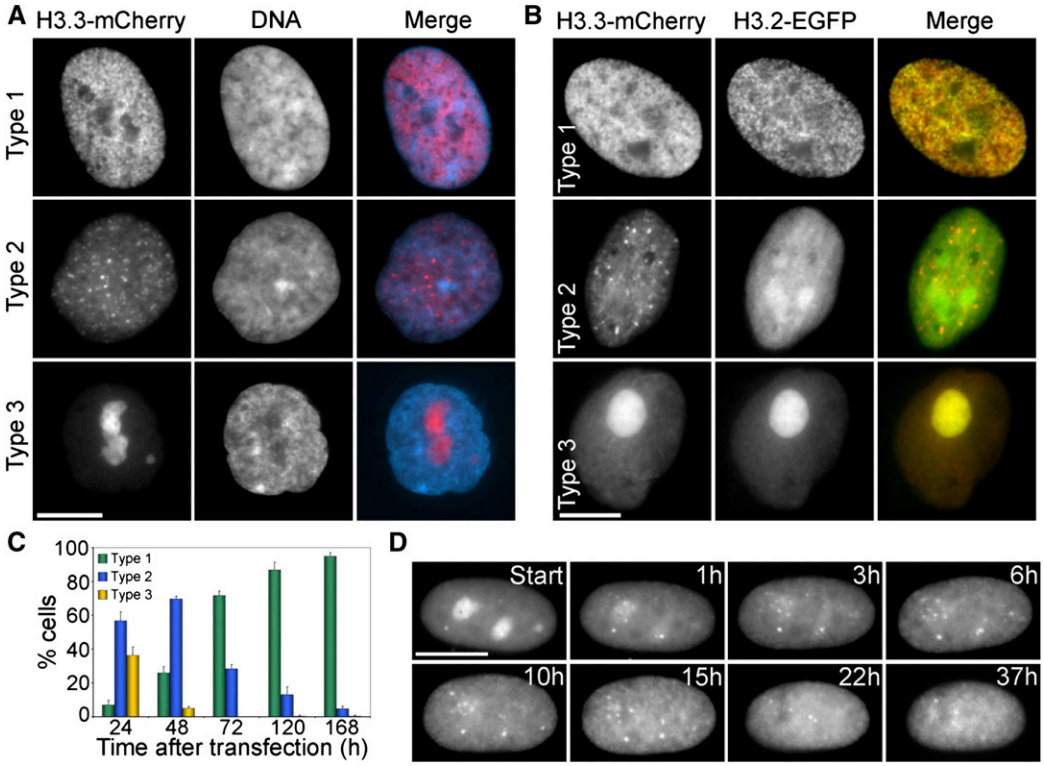

Figure 1. Sequential targeting of epitope-tagged H3.3 to chromatin. (*A*) Intranuclear localization of H3.3-mC 24 h after transient transfection. (*B*) Intranuclear localization of H3.3-mC and H3.2-EGFP after cotransfection as in *A*. (*C*) Percentage of cells shown in *A* displaying indicated H3.3-mC distribution patterns over time after transfection (mean ± SD of three experiments, with more than 120 cells analyzed per experiments). (*D*) Time-lapse imaging of H3.3-mC starting 24 h after transfection (see Supplemental Movie 1). Scale bars, 10 μm.

These include (1) a "type 1" pattern colocalizing with DNA, which we have previously shown by salt and DNase I extraction corresponds to exogenous H3.3 incorporated into chromatin (Delbarre et al. 2010); (2) distinct intranuclear foci, or nuclear bodies (NBs; "type 2"), excluded from heterochromatin regions and resistant to in situ extraction with 0.1% Triton X-100 and 1 M NaCl (Supplemental Fig. 1A); and (3) enrichment in nucleoli ("type 3"). The same distribution patterns are observed with EGFP-tagged H3.3 expressed alone or together with H3.3-mC (Supplemental Fig. 1B), and these are independent of expression level (Supplemental Fig. 1C). In contrast to H3.3, canonical core histone H2B-EGFP decorates chromatin irrespective of H3.3-mC distribution (Supplemental Fig. 1D), suggesting a distinct chromatin deposition pathway. H3.1 or H3.2 tagged with EGFP or mC displays nucleolar, nucleoplasmic, and chromatin enrichment; however, intranuclear foci are not observed (Fig. 1B; Supplemental Fig. 1E). Thus, among histones examined so far, the detection of type 2 NBs appears to be specific for H3.3.

Quantification of the proportion of each H3.3-mC pattern over time after transfection reveals a sequential dominance of enrichment in nucleoli and NBs (type 3/type 2), NBs (type 2), and chromatin (type 1) (Fig. 1C). To demonstrate sequential enrichment of H3.3-mC in these structures, we carried out time-lapse video microscopy of H3.3-mC, and reveal redistribution from nucleoli to NBs and chromatin (Fig. 1D; Supplemental Movie 1). We conclude that epitope-tagged H3.3 follows a stepwise enrichment in nucleoli, discrete NBs, and chromatin.

H3.3 colocalizes with the H3.3 chaperones DAXX, ATRX, HIRA, and ASF1A at PML bodies

Assembly of (H3–H4) dimers into nucleosomes is mediated by chaperones, among which HIRA, ATRX, and DAXX are specific for H3.3, while ASF1A has been proposed to function differentially in replication-dependent and independent assembly of H3 variants into chromatin (Tagami et al. 2004; Groth et al. 2005; Galvani et al. 2008). Remarkably, we find that H3.3-mC NBs colocalize with each of these chaperones (Fig. 2A; Supplemental Fig. 2A). Moreover, H3.3-mC NBs overlap with PML bodies (Fig. 2A; Supplemental Fig. 2A), which we show is consistent with the colocalization of DAXX and ATRX with PML in cells not overexpressing H3.3 (Supplemental Fig. 2B; see also Xue et al. 2003; Tang et al. 2004). Importantly, subpopulations of cells show colocalization of PML with HIRA (27% ± 1%) (Fig. 2B,C) and with ASF1A (5% ± 2%) (Fig. 2B,C)

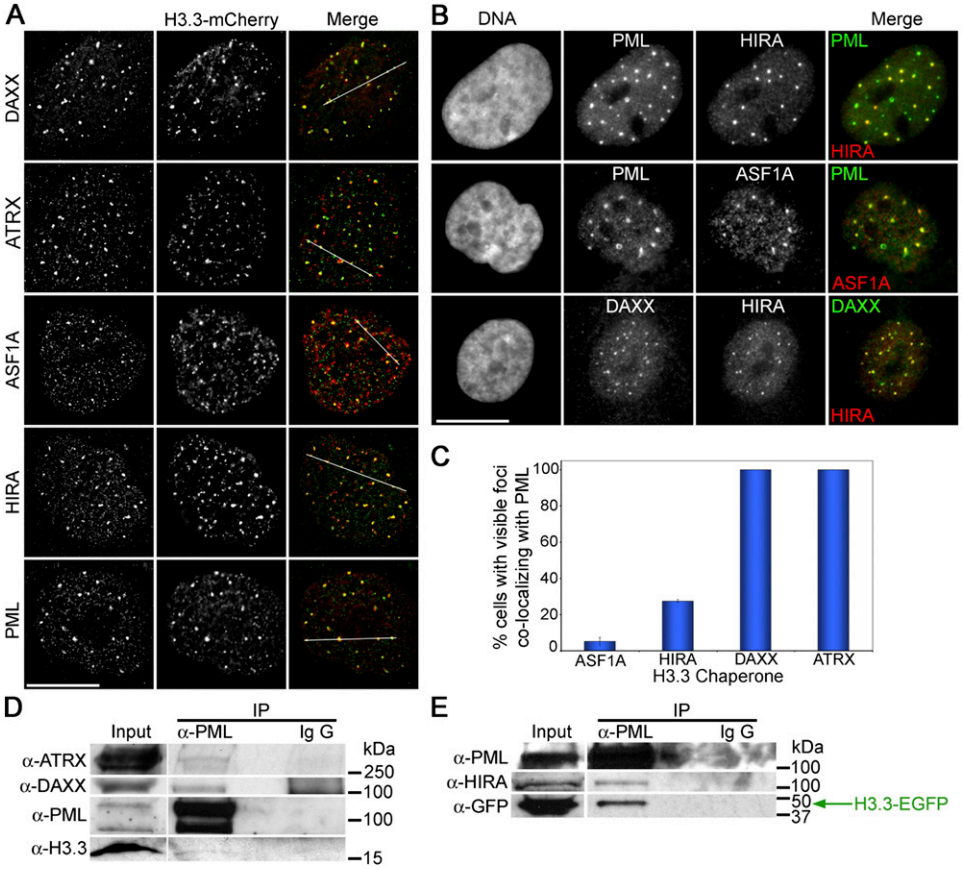

Figure 2. Epitope-tagged H3.3 and H3.3 chaperones are co-enriched at PML bodies. (*A*) Immunolocalization of DAXX, ATRX, HIRA, ASF1A, and PML in NBs, together with H3.3-mC (24 h after H3.3-mC transfection; deconvoluted images). In merged images, red is for H3.3-mCherry and green is for immunostainings. White lines in merged images delineate the zone of fluorescence signals quantified in Supplemental Figure 2A. (*B*) Immunolocalization of PML, HIRA, ASF1A, and DAXX at NBs in nontransfected cells. Scale bars, 15 μm. (*C*) Percentage of cells with NBs of ASF1A, HIRA, DAXX, and ATRX colocalizing with PML (mean ± SD of three countings in independent cell populations, with more than 300 cells per counting). (*D*) Coimmunoprecipitation of ATRX, DAXX, and endogenous H3.3 with PML, using anti-PML antibodies. (*E*) Coimmunoprecipitation of HIRA and H3.3-EGFP (detected with anti-GFP antibodies) with PML, using anti-PML antibodies, from cells overexpressing H3.3-EGFP (24 h after transfection).

in the absence of exogenous H3.3, and PML bodies colocalizing with ASF1A also overlap with HIRA (Supplemental Fig. 2C). Of note, the lack of β-galactosidase reactivity and the proliferative state of the cells used in our study indicate that colocalization of ASF1A or HIRA with PML is not a result of senescence as suggested previously (Zhang et al. 2005; Rai et al. 2011). Therefore, enrichment of ATRX, DAXX, HIRA, and ASF1A in NBs and their colocalization with PML do not result from H3.3 overexpression. Interestingly, HIRA and DAXX NBs colocalize (Fig. 2B) despite the reported partitioning of these chaperones into biochemically distinct complexes (Drane et al. 2010; Goldberg et al. 2010).

Double immunolabeling indicates that H3.3-mC does not overlap with the pericentric chromatin marker CENPA, another H3 variant, or the telomeric protein TRF2 (Supplemental Fig. 2D). This is consistent with the lack of PML detection in pericentric and telomeric chromatin in the somatic cells examined here (Supplemental Fig. 2E), unlike in embryonic stem cells (Wong et al. 2009), and suggests differences in nucleosome turnover rate in these repeat regions in pluripotent versus nonpluripotent cells. We conclude that shortly after induction of expression, epitope-tagged H3.3 is enriched together with DAXX, ATRX, HIRA, and ASF1A at PML bodies, but not at centromeres or telomeres. These results suggest therefore an accumulation of H3.3 at PML bodies prior to deposition into chromatin.

Colocalization of epitope-tagged H3.3 and H3.3 chaperones with PML raises the possibility that these proteins interact in the PML compartment. To test this possibility, we immunoprecipitated PML using anti-PML antibodies. Our data show that DAXX and ATRX coprecipitate with PML (Fig. 2D). DAXX also coprecipitates with a transiently expressed EGFP-PML (isoform V) construct (Supplemental Fig. 2F), consistent with a recent study showing that the C terminus of this isoform recruits DAXX into NBs in MEFs (Geng et al. 2012). Furthermore, both endogenous H3.3 (Fig. 2D; from nontransfected cells) as well as H3.3-EGFP (Fig. 2E) are detected in these immune precipitates. HIRA and ASF1A do not distinctively coprecipitate with PML using PML antibodies in nontransfected cells (data not shown), consistent with the fact that these proteins colocalize with PML bodies only in a subpopulation of cells (see above). However, HIRA coprecipitates together with PML and H3.3-EGFP in H3.3-EGFP-expressing cells (Fig. 2E), suggesting that accumulation of H3.3-EGFP to PML bodies stimulates its association with HIRA in these structures. These results indicate that H3.3, together with at least DAXX, ATRX, and HIRA, are in one or several interacting complexes at PML bodies. This is consistent with a view of H3.3 being able to partner with these different chaperones in PML bodies.

H3.3 recruitment to PML bodies is facilitated by histone H4

Histone H4 is the main partner of all H3 isoforms in the nucleosome, and (H3–H4) dimerization is required for H3.3 and H4 deposition into chromatin. Thus, H4 synthesis during S phase would be expected to facilitate the formation of (H3.3–H4) dimers and tetramers, and their deposition into chromatin. We examined the effect of H4 coexpression on the distribution of epitope-tagged H3.3, H3.2, and H3.1. Expression of mC-H4 or EGFP-H4 alone results in a similar distribution pattern as epitope-tagged H3.3, yet with a faster incorporation time course (Fig. 1A,C; Supplemental Fig. 3A,B), and mC-H4 NBs also colocalize with PML bodies (Supplemental Fig. 3C). This strongly suggests that exogenous H4 associates with endogenous H3.3. Moreover, coexpression of H4 with any of the three H3 variants abolishes nucleolar enrichment detected for exogenous H3 or H4 when these are expressed alone (Fig. 3A; Supplemental Fig. 3D,E), suggesting that this accumulation is caused by altered stoichiometry between H3 and H4 available to form dimers or tetramers. Coexpression of H4 and H3.3 also leads to complete overlap of both proteins in type 2 NBs (Fig. 3A). Cells coexpressing H4 and H3.1 or H3.2 also display H4 NBs; however, these do not overlap with these H3 variants (Supplemental Fig. 3D,E). In addition, coexpression of H4 and H3.3 accelerates the deposition of H3.3-mC into chromatin (Fig. 3B; cf. Fig. 1C), where both proteins also overlap (Fig. 3A). These results argue that exogenous H3.3 requires association with H4 to exit the nucleolar compartment, and that H3.3 and H4 are driven together to PML bodies. However, one cannot thus far exclude that association of H3.3 and H4 occurs at PML bodies.

To evaluate a role of H4 in directing H3.3 to PML bodies, we assessed the mobility of H3.3-EGFP at NBs with or without expression of exogenous H4, by fluorescence recovery after photobleaching (FRAP) of H3.3-EGFP. We photobleached H3.3-EGFP in chromatin (Supplemental Fig. 3F, upper panels), and reveal <20% EGFP fluorescence recovery in the bleached area within 30 min (Fig. 3C, red line), indicating that this H3.3-EGFP pool is stably incorporated into chromatin. A similar result was obtained with H2B-EGFP (Fig. 3C, yellow line), as expected for a canonical core

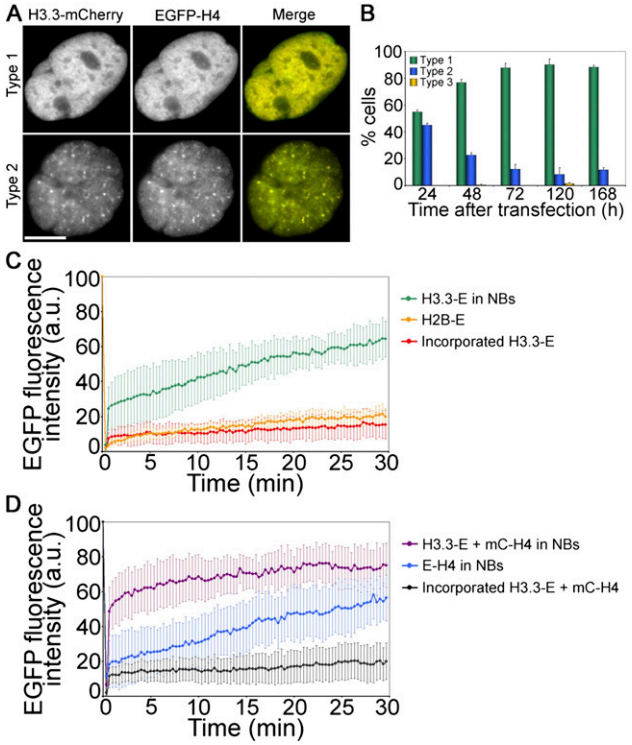

Figure 3. Expression of histone H4 accelerates the targeting of H3.3 to nuclear bodies and chromatin. (*A*) Colocalization of H3.3-mC and EGFP-H4 in NBs (type 2) and in chromatin (type 1). Scale bars, 10 μm. (*B*) Time course of detection of type 1, 2, and 3 H3.3-mC patterns after cotransfection with EGFP-H4 (mean ± SD of three experiments with more than 120 cells analyzed per experiment). (*C*) FRAP analysis of H3.3-EGFP (H3.3-E) in NBs or after incorporation into chromatin. The fluorescence recovery of chromatin-incorporated canonical core histone H2B-EGFP is shown as control (mean ± SD of seven to eight cells). (*D*) FRAP analysis of H3.3-EGFP in NBs or incorporated into chromatin in cells coexpressing mC-H4, and in cells expressing EGFP-H4 alone in NBs (mean ± SD of eight to 10 cells).

histone (Kimura 2005). Next, we bleached H3.3-EGFP at NBs (Supplemental Fig. 3F, middle panels); this resulted in a marked recovery (>60% within 30 min) of EGFP fluorescence at these sites (Fig. 3C, green line). Therefore, H3.3-EGFP is significantly more mobile at NBs, revealing a predominant exchanging pool of H3.3 at these sites. To determine whether H3.3-EGFP NBs bleached in these experiments correspond to PML bodies, we coexpressed mCherry-tagged PML and H3.3-EGFP, and photobleached H3.3-EGFP at foci illuminated by mCherry. H3.3-EGFP fluorescence recovery in these cells is similar to that of H3.3-EGFP NBs in cells not overexpressing mC-PML (see below). Thus, recovery of H3.3-EGFP fluorescence measured at NBs occurs at PML bodies. In addition, photobleached EGFP-H4 decorating NBs shows similar fluorescence recovery to H3.3-EGFP at these sites (Fig. 3D, blue line), consistent with a similar recruitment pattern of H3.3 and H4 to NBs.

Lastly, to determine whether H4 affects H3.3 dynamics at NBs, we coexpressed mC-H4 and H3.3-EGFP and show that mC-H4 expression accelerates recovery of bleached H3.3-EGFP at NBs (cf. Fig. 3D, purple line, with Fig. 3C, green line; Supplemental Fig. 3F). Within 1 min after photobleaching, expression of mC-H4 elicits 54.8% ± 13.3% fluorescence recovery compared with 21.0% ± 7.9% when H3.3-EGFP is expressed alone ($P = 0.0002$) (Fig. 3C,D). Importantly, mC-H4 expression does not affect fluorescence recovery of H3.3-EGFP in the chromatin compartment (Fig. 3D, black line; cf. Fig. 3C, red line), demonstrating incorporation of H3.3 and H4 into chromatin.

Collectively, these results indicate that H4 overexpression elicits faster recruitment of H3.3-EGFP to NBs and infer that H4 availability influences H3.3 mobility at these sites. This is consistent with the view that H3.3 and H4 associate prior to targeting to PML bodies, and that exit of H3.3 from PML bodies also requires association with H4.

DAXX but not ATRX recruits H3.3 to PML bodies

The colocalization of DAXX and ATRX with H3.3 and PML bodies (this study), the known interaction between these two chaperones and H3.3 (Drane et al. 2010; Goldberg et al. 2010; Lewis et al. 2010; Wong et al. 2010), and the coimmunoprecipitation of DAXX, ATRX, and H3.3 with PML (this study), raise the possibility that either chaperone may promote H3.3 recruitment to PML bodies. To address this issue, we depleted DAXX and ATRX using siRNAs (Supplemental Fig. 4A) and show by immunoblotting that DAXX depletion does not affect the level of ATRX, and vice versa (Fig. 4A). However, using two different siRNAs, we show that DAXX depletion causes a redistribution of ATRX in the nucleus, with the disappearance of discrete ATRX NBs (Fig. 4B,C; Supplemental Fig. 4B; see also Ishov et al. 2004). In contrast, ATRX depletion maintains DAXX at PML bodies (Fig. 4B; Supplemental Fig. 4B). Therefore, localization of ATRX at PML bodies depends on DAXX, but DAXX localizes with PML independently of its association with ATRX. Neither ATRX nor DAXX knockdown prevents the formation of PML bodies (Fig. 4B; Supplemental Fig. 4B) or their association with HIRA or ASF1A NBs (Supplemental Fig. 4C–F). Thus, formation of PML bodies and association of ASF1A and HIRA with PML are independent of the DAXX/ATRX complex.

To assess the role of DAXX and ATRX in recruiting H3.3 to PML bodies, we independently depleted DAXX and ATRX by siRNA in cells expressing H3.3-mC. To this end, we first down-regulated DAXX or ATRX with siRNAs to near depletion, and after 4 d, expressed H3.3-mC simultaneously to a second round of

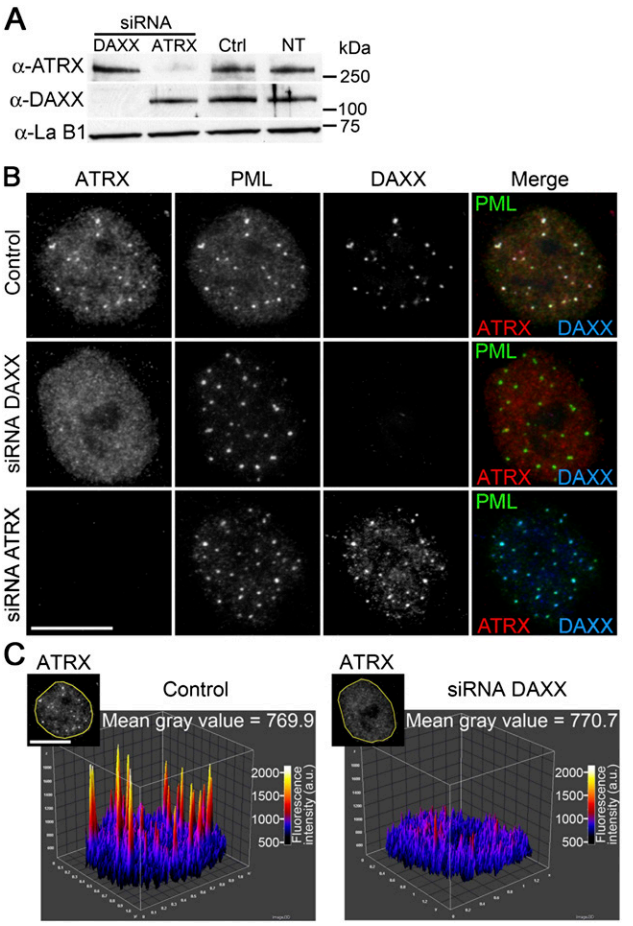

Figure 4. DAXX down-regulation delocalizes ATRX from PML bodies. (*A*) Western blot analysis of siRNA-mediated ATRX and DAXX down-regulation. Lamin B1 is shown as loading control. (Ctrl) Control sham depletion with H_2O; (NT) nontransfected cells. (*B*) Immunolocalization of ATRX, PML, and DAXX in sham-depleted (*top*), DAXX-depleted (*middle*), and ATRX-depleted (*bottom*) cells. (C) Distribution of ATRX in a sham (control)– and DAXX-depleted cell (shown in *inset*, corresponding to ATRX pictures in panel *A*). ATRX-associated fluorescence intensity of each pixel delimited by the yellow line in *insets* is plotted in a three-dimensional graph. The similarity of the mean gray values in both cell types shows that relocalization of ATRX in DAXX-depleted cells is not due to a lower amount of fluorescence signal. Scale bars, 15 μm.

siRNA transfection to maintain the depletion of DAXX or ATRX. DAXX depletion results in redistribution of H3.3-mC 24 h after H3.3-mC transfection, with much less prominent NBs, poorly colocalizing with PML (Fig. 5A,B). Conversely, overexpression of DAXX-mC together with H3.3-EGFP leads to a robust overlap of the two proteins at PML bodies (Fig. 5C). In contrast, ATRX depletion maintains the localization of H3.3-mC at PML bodies (Fig. 5D). Altogether, these results argue that DAXX, but not ATRX, plays a role in recruiting H3.3 to PML bodies.

We next determined by FRAP whether DAXX and ATRX depletion would alter the mobility of H3.3. We show that, using two different siRNAs, DAXX silencing strongly reduces targeting of H3.3-EGFP to the photobleached remaining foci (Fig. 5E, blue, purple, and green lines). This is also observed in cells coexpressing H3.3-EGFP and mC-PML (Supplemental Fig. 5). Conversely, overexpression of DAXX dramatically enhances recruitment of H3.3-EGFP to NBs, with foci already visible within the first 20 sec

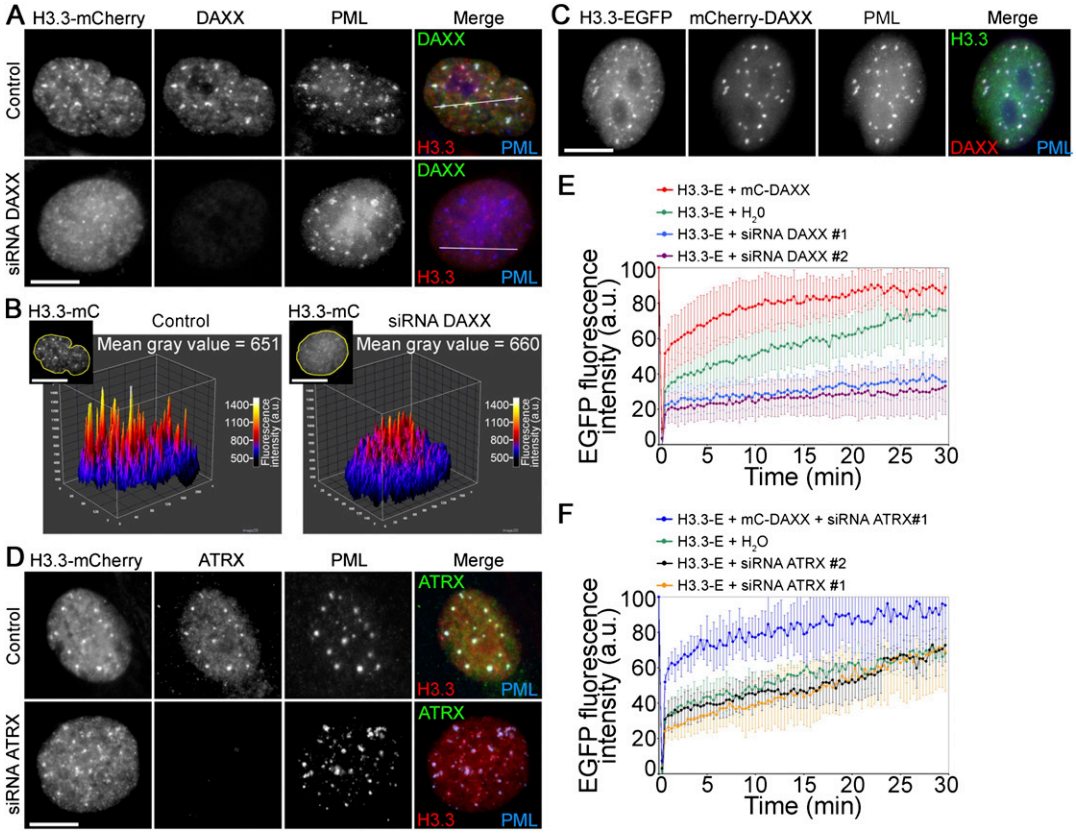

Figure 5. Down-regulation of DAXX, but not ATRX, abolishes recruitment of H3.3 to PML bodies. (*A*) Immunolocalization of DAXX and PML in cells expressing H3.3-mC, after sham (control) or siRNA-mediated DAXX knockdown. (*B*) Distribution of H3.3-mC fluorescence in a sham (control)– and DAXX-depleted cell (shown in *inset*, corresponding to H3.3-mCherry pictures in *A*). (*C*) Colocalization of coexpressed H3-3-EGFP and mC-DAXX with immunolabeled PML. (*D*) Immunolocalization of ATRX and PML in cells expressing H3.3-mC, after sham (control) or siRNA-mediated ATRX knockdown. (*E*) FRAP analysis of H3.3-EGFP in cells expressing mC-DAXX, in cells depleted of DAXX using two different siRNAs, and in sham-depleted cells (H_2O) (mean ± SD of 10–14 cells). (*F*) FRAP analysis of H3.3-EGFP in ATRX-depleted (using two different siRNAs) and sham (H_2O)–depleted cells, and in cells expressing mC-DAXX and depleted of ATRX (mean ± SD of seven cells). Scale bars, 10 μm.

after photobleaching (Fig. 5E, red line). In contrast to DAXX silencing, ATRX silencing does not affect H3.3-EGFP recovery at NBs after photobleaching (Fig. 5F, green, black, and yellow lines), even after overexpression of DAXX (Fig. 5F, blue line; cf. Fig. 5E, red line). This confirms that ATRX does not play a significant role in recruiting H3.3 to PML bodies. Collectively, these results show that DAXX is involved in the recruitment of H3.3 to PML bodies.

DAXX prevents accumulation of soluble H3.3 in the nucleoplasm

Since DAXX recruits a soluble pool of H3.3–H4 to PML bodies, we next determined whether the amount of unincorporated epitope-tagged H3.3 several days after transfection was affected by the absence of DAXX. After 4 d of H3.3 expression, when H3.3 is expected to be incorporated into chromatin (see Fig. 1C), a large majority of siRNA DAXX-treated cells display a distribution pattern similar to incorporated H3.3-EGFP, comparable to control cells (see Fig. 1A,C). However, FRAP analysis shows that DAXX depletion induces greater recovery of H3.3-EGFP (29.8% ± 7.9%) than sham-depleted cells (10.5% ± 6.3%, $P = 0.008$) within the first 5 min after photobleaching (Fig. 6A), corresponding to a larger pool of highly mobile nucleoplasmic H3.3-EGFP. To confirm the soluble nature of this pool, we extracted these DAXX-depleted cells with 1% Triton X-100 to separate soluble (cytosolic and nucleoplasmic) and insoluble fractions. As expected, most H3.3-EGFP was insoluble in control and DAXX-depleted cells; however, a significant pool of H3.3-EGFP was also identified in the soluble fraction only after DAXX depletion (Fig. 6B). Thus, the absence of DAXX promotes the retention of a soluble pool of H3.3 that is not incorporated into chromatin. These results suggest that DAXX prevents the accumulation of soluble H3.3 by promoting its targeting to insoluble compartments such as PML bodies or chromatin.

PML bodies are sites of recruitment of H3.3 not incorporated to chromatin

We have earlier shown that in addition to H3.3, DAXX, ATRX, and HIRA are in one or more complexes at PML bodies. To demonstrate a role of PML in the congregation of H3.3 and chaperones at these sites, we knocked down PML by siRNA and assessed by imaging the localization of H3.3-EGFP and the chaperones. Depletion of PML results in the redistribution of H3.3, DAXX, ATRX, HIRA, and ASF1A (Fig. 6C; Supplemental Fig. 6A–D). We nonetheless note rare DAXX foci, despite the disappearance of PML, which coincide with ATRX, but not HIRA or ASF1A. To independently demonstrate a role of PML bodies in locally concentrating H3.3 and chaperones, PML bodies were disrupted with 2 μM AS_2O_3. This resulted in the

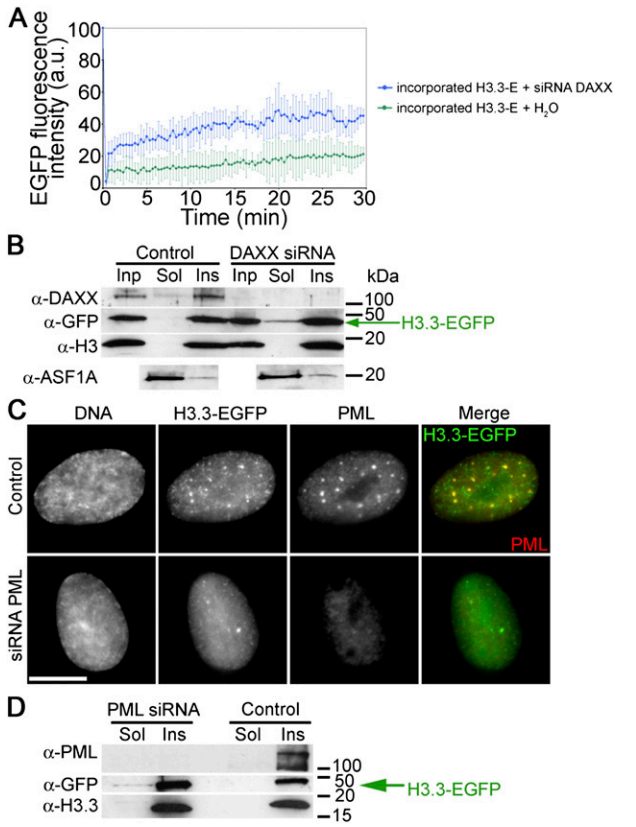

Figure 6. DAXX down-regulation generates a soluble pool of H3.3. (*A*) FRAP analysis of H3.3-EGFP incorporated into chromatin in DAXX- and sham (H_2O)–depleted cells 96 h after transfection (mean ± SD of five cells). (*B*) Western blot analysis of H3.3-EGFP distribution in DAXX- and sham (control)–depleted cells. Cell lysates (Inp, input) were fractionated into 1% Triton X-100 soluble (sol) and insoluble (Ins) fractions. H3.3-EGFP is detected with anti-GFP antibodies. H3 is shown as a chromatin marker. ASF1A is shown as a marker of the soluble fraction. (*C*) Redistribution of H3.3-EGFP after siRNA-mediated knockdown of PML. (*D*) Western blot analysis of H3.3-EGFP distribution in Triton X-100 soluble and insoluble fractions, from PML- and sham (control)–depleted cells. Cell lysates were fractionated as in *B*.

disappearance of PML bodies, interpreted as their dismantlement, with nevertheless occasional remaining large PML protein aggregates (Supplemental Fig. 6E–H). Whereas in the remaining structures DAXX, HIRA, ASF1A, and H3.3-mCherry could be detected, disruption of PML bodies results in the dispersion of the chaperones and H3.3 (Supplemental Fig. 6E–H). We conclude that PML bodies constitute sites of anchoring of H3.3 that is not incorporated into chromatin, together with DAXX, ATRX, HIRA, and ASF1.

If PML bodies are important for DAXX-mediated incorporation of H3.3 into insoluble structures, depletion of PML would also be expected to increase the pool of soluble H3.3. To address this, PML was down-regulated by siRNA in cells expressing H3.3-EGFP and after 4 d of H3.3-EGP expression, cells were extracted with 1% Triton X-100 as above to separate soluble and insoluble fractions. The data show that PML depletion also leads to a soluble pool at H3.3-EGFP that is not detectable in control cells (Fig. 6D). Thus, as DAXX, PML bodies play a role in the prevention of accumulation of a soluble reservoir of H3.3.

The results from these and the previous experiments support a role of DAXX and PML in targeting H3.3 to insoluble NBs or chromatin. They are consistent with a model of PML bodies as a meeting point for H3.3 together with DAXX, ATRX, HIRA, and ASF1A before deposition into chromatin.

DAXX preferentially targets H3.3–H4 to PML bodies as dimers rather than tetramers

Targeting of H3.3 to PML bodies from a soluble pool together with H4 (see Fig. 3A) raises the question of whether this recruitment occurs in the form of (H3–H4) dimers or $(H3–H4)_2$ tetramers. To distinguish between these alternatives, we generated an H3.3 mutant in which His113 substitution with Ala (H3.3[H113A]) allows, in silico, H3–H4 dimerization but prevents the formation of stable $(H3–H4)_2$ tetramers by disrupting the H3–H3′ hydrogen bond (Ramachandran et al. 2011). H3.3(H113A)-mC colocalizes at foci with PML 24 h after transfection (Fig. 7A). FRAP analysis of these H3.3(H113A)-EGFP foci reveals faster and greater recovery of H3.3(H113A) than H3.3 (Fig. 7B, red and green lines), and recovery at these foci is abolished in DAXX-depleted cells (Fig. 7B, yellow and blue lines). Of note, we observe within the first 20 sec after photobleaching a significant recovery of fluorescence (36.8% ± 10%) (Fig. 7B, yellow line), which we show occurs at the level of the nucleoplasmic soluble pool of H3.3(H133A)-EGFP surrounding foci in the bleached area (Supplemental Fig. 7A, lower panel). However, fluorescence recovery specifically at the foci is inhibited (Supplemental Fig. 7A, lower panel). These results indicate that DAXX can recruit both H3.3 and H3.3(H113A) to PML bodies, and suggest that (H3.3–H4) is recruited to PML by DAXX preferentially as a dimer rather than as a tetramer.

ASF1A has been shown to bind free (H3–H4) dimers and proposed to disrupt $(H3–H4)_2$ tetramers (English et al. 2006; Groth et al. 2007; Natsume et al. 2007; Elsasser et al. 2012). Thus, if our hypothesis of recruitment of (H3.3–H4) to PML as dimers is correct, overexpression of ASF1A should facilitate H3.3 recruitment to PML as a result of a shift in the stoichiometry of (H3–H4) dimers and $(H3–H4)_2$ tetramers toward the formation of dimers. To test this possibility, we coexpressed ASF1A-mC and H3.3-EGFP and assessed H3.3-EGFP recovery at NBs after photobleaching. We observe by FRAP faster fluorescence recovery of H3.3-EGFP at NBs than in control cells (cf. Fig. 7C, black line; Fig. 7B, green line), and this recovery is mediated by DAXX (Fig. 7C, yellow and pink lines). Again, we detect a highly mobile fraction of H3.3-EGFP in DAXX-depleted cells in the presence of ASF1A-mC corresponding to a soluble pool of H3.3 surrounding the NBs (43.2% ± 10.6% recovery within 20 sec of photobleaching) (Fig. 7C, pink line). These results indicate that ASF1A facilitates DAXX-mediated recruitment of H3.3 to PML but is not directly involved in H3.3 targeting to these sites. To confirm this, we down-regulated ASF1 by siRNA (Supplemental Fig. 7B) in cells overexpressing DAXX, and show by FRAP a fluorescence recovery of H3.3-EGFP at NBs with a kinetics similar to those observed in ASF1A-containing control cells (Supplemental Fig. 7C). Collectively, these results show that recruitment of H3.3 by DAXX to PML bodies preferentially occurs in the form of (H3.3–H4) dimers. This recruitment is facilitated by ASF1A, which increases the availability of (H3–H4) dimers in the nucleoplasm.

Discussion

We report here the recruitment of newly synthesized epitope-tagged H3.3 to PML bodies prior to deposition into chromatin. Our results provide several new insights into the chromatin deposition

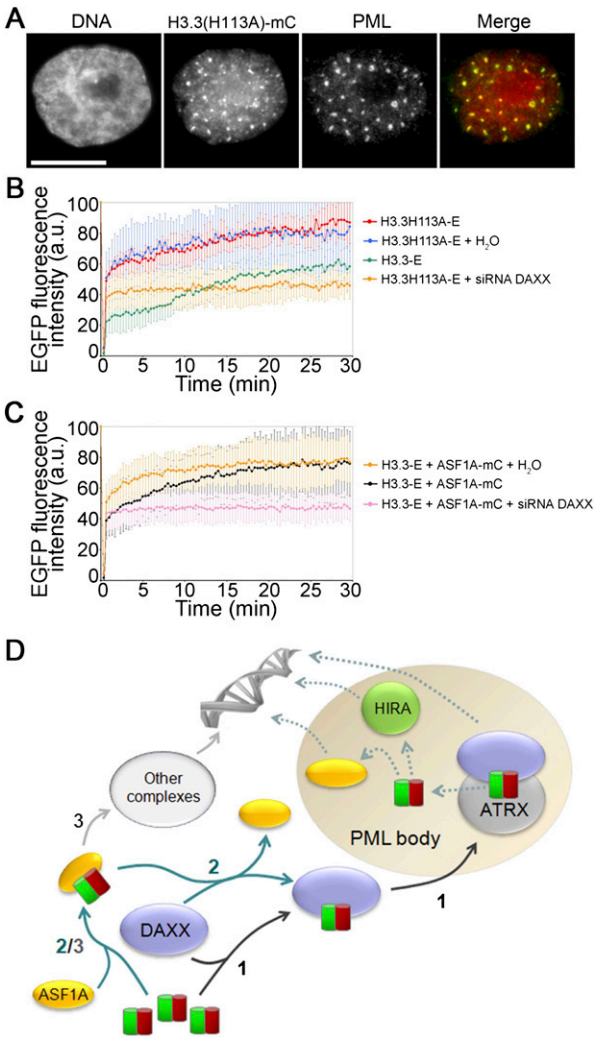

Figure 7. Accelerated recruitment of an $(H3.3–H4)_2$ tetramerization mutant to PML bodies. (*A*) Colocalization of an H3.3(H113A)-mC tetramerization mutant with immunolabeled PML, 24 h after transfection. (*B*) FRAP analysis of H3.3(H113A)-EGFP in NBs with and without siRNA-mediated down-regulation of DAXX. H3.3-EGFP recovery was examined in parallel as control. H3.3(H113A)-EGFP displays a greater soluble pool than H3.3-EGFP, and recovery at NBs is abolished by DAXX knock-down (see Supplemental Fig. 7A for fluorescence recovery of the soluble fraction and at NBs) (mean±SD of 7-14 cells). (*C*) FRAP analysis of H3.3-EGFP in NBs in cells expressing ASF1A-mC with or without siRNA-mediated DAXX knock-down (mean±SD of 10-17 cells). (*D*) Model of (H3.3–H4) dimer recruitment to PML bodies prior to chromatin deposition. In pathway 1, DAXX recruits the (H3.3–H4) dimer to PML bodies. This process is facilitated by ASF1A (pathway 2). (H3.3–H4) loaded onto ASF1A can also be brought to additional H3.3 chaperone containing complexes (Szenker et al. 2011) (pathway 3). DAXX, ATRX, HIRA, and ASF1A are localized in a proportion of PML bodies and may speculatively be available for loading (H3.3–H4) prior to deposition into chromatin (dashed arrows).

pathway of H3.3 into chromatin. We show a dynamic process involving a nucleolus–PML body–chromatin axis for at least a fraction of H3.3. We demonstrate a specific role of DAXX, independently of ATRX, in the recruitment of H3.3 to PML bodies, in a process that can be facilitated by ASF1A. This recruitment occurs as (H3.3–H4) dimers rather than as tetramers. Moreover, and most importantly, we provide evidence for a hitherto unknown function of PML bodies in the targeting of H3.3 to chromatin: (1) identification of four chaperones specific for H3.3, namely, DAXX, ATRX, HIRA, and ASF1A, together with H3.3 in PML bodies; (2) biochemical interactions of PML with H3.3 and H3.3 chaperones; and (3) accumulation of a soluble pool of H3.3 after depletion of PML (or DAXX) altogether suggest a model of triage of newly synthesized H3.3 to multiple chaperones in PML bodies before deposition into chromatin.

We have in this study taken advantage of a transient transfection strategy to induce expression of epitope-tagged H3.3, in a primary human cell type with a long G_1 phase (91% of the cells used here are in G_1 in an unsynchronized population) (Gaustad et al. 2004). This enables identification of epitope-tagged H3.3 localization intermediates before deposition into chromatin, in the absence of potentially perturbing chemical synchronization. We show that epitope-tagged H3.1, H3.2, H3.3, or H4, when expressed alone, first accumulate in nucleoli; this may be a result of transient overexpression of these proteins. However, because H4 coexpression with any of these H3 isoforms abolishes this phenotype, nucleolar accumulation is likely due to altered stoichiometry between H3 and H4 dimerization partners. Nucleolar targeting of H3.3 may nevertheless not preclude a physiological role of H3.3 in nucleoli after chromatin incorporation has taken place. A fraction of H3.3 is retained at foci in nucleoli even after bulk H3.3 is incorporated into chromatin (E Delbarre and P Collas, unpubl.). This H3.3 fraction may be associated with ribosomal DNA, as shown in *Drosophila* cells (Ahmad and Henikoff 2002) and in *Arabidopsis* (Shi et al. 2011). Detection of ATRX at pericentric heterochromatin of human acrocentric chromosomes (McDowell et al. 1999; Gibbons et al. 2000), which in interphase is concentrated in nucleoli, is consistent with a role of H3.3 with ribosomal gene expression.

It should be mentioned that transient expression of nuclear proteins may induce their detection at sites that otherwise might not be readily visible with their endogenous counterparts. This may potentially be due to (1) inaccessibility of antigens to antibodies in dense nuclear structures such as PML bodies; (2) epitope masking, such as for H3.3, coverage with DAXX (Elsasser et al. 2012) or ATRX (Eustermann et al. 2011; Iwase et al. 2011); or (3) accumulation of only a minor pool of endogenous H3.3 in these structures under normal conditions. We nonetheless observe a transition of epitope-tagged H3.3 from nucleoli to NBs and to chromatin, not seen for H3.1 or H3.2. This argues for a pathway-specific H3.3 rather than a mere result of protein overexpression.

DAXX targets (H3.3–H4) dimers to PML bodies

Our demonstration of DAXX-dependent recruitment of exogenous H3.3 to PML bodies is consistent with previous work showing that DAXX overexpression induces accumulation of H3.3-EGFP at PML in $Daxx^{-/-}$ ES cells (Drane et al. 2010). DAXX and ATRX are part of a same complex that associates with H3.3 (Drane et al. 2010; Goldberg et al. 2010; Lewis et al. 2010). Since ATRX itself binds H3.3 (Eustermann et al. 2011; Iwase et al. 2011), detection of H3.3 at PML in mouse embryonic stem cells (Drane et al. 2010) could be due to ATRX recruitment to PML by DAXX (Tang et al. 2004). We now demonstrate that DAXX mediates H3.3 recruitment to PML bodies independently of ATRX.

Our findings of faster PML targeting of a mutant of H3.3 (H3.3[H113A]) that has computationally been found to abolish the formation of $(H3.3–H4)_2$ tetramers (Ramachandran et al. 2011) suggest a model in which DAXX recruits (H3.3–H4) dimers rather

than tetramers to PML bodies. The H113A substitution disrupts hydrogen bonding and hydrophobic interactions of H113 with a negatively charged pocket formed by the adjacent H3 surface. Thus, it abolishes H3–H3′ interactions and $(H3–H4)_2$ tetramer assembly. Because DAXX displays rapid turnover at PML bodies in cell lines (Weidtkamp-Peters et al. 2008) and colocalizes with PML in nontransfected primary cells (this study), we propose that DAXX recruits endogenous (H3.3–H4) dimers to PML bodies in normal primary cells. Previous studies show that DAXX is able to promote deposition of (H3.3–H4) into chromatin (Drane et al. 2010; Lewis et al. 2010; Elsasser et al. 2012). Our data now implicate a role of PML bodies in (H3.3–H4) chromatin incorporation, and imply that part of the function of DAXX in eliciting H3.3 deposition may be mediated through PML. These observations altogether underline a putative dual role of DAXX: DAXX may promote recruitment of (H3.3–H4) to PML bodies, as well as enable deposition of (H3.3–H4) into chromatin. Whether recruitment of (H3.3–H4) dimers to PML bodies is necessary for DAXX-mediated deposition into chromatin remains to be investigated.

HIRA and ASF1A accumulate at PML bodies independently of DAXX and ATRX

HIRA and ASF1A have been shown to associate with PML bodies in primary cells entering senescence, but not in cycling and transformed cells (Zhang et al. 2005; Jiang et al. 2011). Our data show HIRA and ASF1A accumulation at PML bodies in a subpopulation of nonsenescent cells; this may nonetheless be due to the low cycling property of the cells used in this study. HIRA and ASF1A detection at PML bodies is independent of DAXX and ATRX, in line with the existence of two distinct H3.3 chaperone complexes (HIRA/CABIN1/UBN1/ASF1A and DAXX/ATRX) (Drane et al. 2010; Goldberg et al. 2010; Lewis et al. 2010; Elsasser et al. 2012). An attractive implication of the association of HIRA, ASF1A, DAXX, and ATRX with PML bodies is a model in which recruitment of (H3.3–H4) dimers to PML bodies by DAXX facilitates association of H3.3 with the different chaperones in these structures acting as a triage center for H3.3, before subsequent deposition into chromatin (Fig. 7D). This would provide an efficient delivery mechanism of nonincorporated (H3.3–H4) dimers to chaperones. A recent study in HeLa cells points to HIRA as a main chaperone involved in neo-synthesized H3.3 deposition into chromatin (Ray-Gallet et al. 2011). Importantly, we show here that H3.3-EGFP overexpression results, early after H3.3-EGFP transfection, in the coprecipitation of HIRA together with PML and H3.3-EGFP; this suggests that accumulation of H3.3-EGFP to PML bodies stimulates its association with HIRA in these structures, supporting a view of PML bodies as chaperone coupling and sorting centers for H3.3. Chromatin incorporation of H3.3 has earlier been assessed based on H3.3 insolubility after Triton X-100 extraction (Ray-Gallet et al. 2002), a finding consistent with chromatin incorporation but also compatible with H3.3 enrichment in PML bodies. Indeed, PML resists nonionic detergents (Stuurman et al. 1992), similarly to NBs decorated by epitope-tagged H3.3 in our present study (Supplemental Fig. 1) and in previous work (Delbarre et al. 2010). Therefore, resistance of H3.3 to Triton X-100 extraction may also partly result from sequestration into PML bodies. It would be informative to determine in the H3.3 detection system of Almouzni and colleagues (Ray-Gallet et al. 2011) the dynamics and subnuclear distribution of neo-synthesized H3.3 immediately after protein expression.

DAXX-dependent recruitment of (H3.3–H4) to PML bodies provides an efficient soluble histone supply mechanism facilitating deposition into chromatin

ASF1A has been shown to play a role in buffering excess soluble (H3.1–H4) dimers under replication stress in HeLa cells (Groth et al. 2005). Even though soluble ASF1A-bound H3.3 was not detected in these cells, this might result from the ability of H3.3 to be incorporated independently of replication (Ahmad and Henikoff 2002). Our results favor a model in which ASF1A facilitates recruitment of H3.3 by DAXX to PML bodies (Fig. 7D, pathway 2). Through its association with (H3–H4) dimers (Elsasser et al. 2012) and disruption of $(H3–H4)_2$ tetramers in vitro (English et al. 2005; Natsume et al. 2007), ASF1A may facilitate the formation of (H3.3–H4) dimers that can be recruited by DAXX. This scenario is compatible with the H3.3 binding motifs for ASF1A and DAXX being distinct (English et al. 2005; Natsume et al. 2007) and with the exclusive association of (H3.3–H4) with ASF1 or DAXX recently explained by crystallography studies (Elsasser et al. 2012). ASF1A is not found in the same H3.3-containing complex as DAXX in pull-down experiments (Drane et al. 2010); however, this is not in contradiction with ASF1A and DAXX being colocalized at PML bodies and found in complex(es) with PML. Association of DAXX with (H3.3–H4) dimers is likely to disrupt their interaction with ASF1A. Since association of H3.3 with HIRA/CABIN1/UBN1/ASF1A may require the formation of an (H3.3–H4)–ASF1A complex (Tang et al. 2012), (H3.3–H4) dimers recruited by DAXX to PML NBs in an ASF1A-facilitated manner might be available to other histone chaperones involved in H3.3 deposition such as HIRA (Fig. 7D). To support this hypothesis, ASF1 has been detected in the HIRA complex (Tagami et al. 2004).

Altogether, the recruitment of H3.3 and ATRX by DAXX to PML bodies and DAXX- and H3.3-independent localization of HIRA and ASF1A to these NBs (Fig. 7) suggest a model of PML bodies as scaffolds integrating H3.3 chaperones, coupled to an accompanying mechanism to funnel (H3.3–H4) dimers. Thus, PML bodies may be perceived as triage centers for a fraction of H3.3 prior to subsequent deposition into specific chromatin domains mediated by distinct histone chaperone complexes. This model opens a new perspective on the functional interdependence of the H3.3 deposition complexes at PML bodies.

Methods

Cells and transfection

Mesenchymal stem cells were purified from human liposuction material from three donors, plated, pooled, and expanded in GlutaMAX (GIBCO) containing 20% fetal calf serum (Boquest et al. 2005). Cells were passaged 1:3 using trypsin-EDTA. Cells at passages 5–15 were used. Transfection was performed with a Nucleofector device (Lonza) in batches of $\sim 4 \times 10^5$ cells mixed with 4 μg of plasmid and/or 200 pmol of siRNA. After electroporation, cells were seeded onto coverslips in 24-well plates for immunofluorescence, in flasks for biochemical extraction, or in 35-mm dishes with a glass bottom (Mattek) for FRAP. For expression of tagged proteins in siRNA-treated cells, a first siRNA transfection was performed followed 96 h later by a second transfection with both siRNA and tagged protein plasmids.

Plasmids and siRNA oligonucleotides

The plasmid encoding ASF1A-mCherry was from Jean-Yves Thuret (CEA Saclay). Plasmids containing mCherry-H4 and EGFP-H4

cDNA were from Maïté Coppey (Institut Jacques Monod, Paris). Plasmids encoding *Drosophila* H3.3 and H3.2 were described in Delbarre et al. (2010). Human DAXX and PML (isoform 5) cDNAs were amplified by polymerase chain reaction (PCR) from plasmids pRK5-Flag-DAXX (gift from David J. Picketts, The Ottawa Health Research Institute, Ottawa, Canada) and pEGFP-PML (gift from Harutaka Katano, National Institute of Infectious Diseases, Toyama, Japan), respectively. For DAXX, the sense primer had an EcoRI site at its 5′ end (5′-GCGAATTCGATGGCCACCGCTAACAGCATCA-3′) and the antisense primer a KpnI site (5′-GCGGTACCTCAATCAG AGTCTGAGAGCACGAT-3′). For PML, the sense primer site had an EcoRI site at its 5′ end (5′-GCGAATTCTATGGAGCCTGCACC CGCCCGA-3′) and the antisense primer a SalI site (5′-GGTGT CGACTCACCACAACGCGTTCCTCCT-3′). The reaction products were digested with the corresponding enzymes and ligated into pEGFP-C1 (Clontech) or pmCherry-C (gift from Maïté Coppey).

Plasmids encoding H3.1-mCherry and H3.3(H113A)-EGFP were made from pH3.3-mCherry and pH3.3-EGFP, respectively, by mutagenesis using the Quick change Site-Directed Mutagenesis Kit (Stratagene) and the following primers: 5′-GCTCTGCAGGAA GCTTGCGAAGCCTACCTG-3′ and 5′-CAGGTAGGCTTCGCAAG CTTCCTGCAGAGC-3′ for H3.1; 5′-ACCAATCTGTGCGCCATTG CCGCCAAGCGCGTCACC-3′ and 5′-GGTGACGCGCTTGGCGG CAATGGCGCACAGATTGGT-3′ for H3.3[H113A].

Sequences of siRNA oligonucleotides were as follows:

ATRX (#1): GAUAUUGCAGAGAAAUUCCUAAAGA
ATRX (#2): AUCAAAGAGGAAACCUUCAAUUGUA
DAXX (#1): GGAGUUGGAUCUCUCAGAAUUGGAU
DAXX (#2): GAUCAUCGUGCUCUCAGACUCUGAU
ASF1A: UAUACUGAGACAGAAUUAAGGGAAA
PML: GGAAGGUCAUCAAGAUGGAGU

Live cell imaging

Cells were kept at 37°C in a humid 5% CO_2 atmosphere and observed on an IX71 inverted microscope (Olympus) fitted with a piezo-driven 100× objective (numerical aperture 1.4) and a CellR wide-field Imaging Station (Olympus). Pictures of the middle plane of the nucleus were acquired every 20 min over several hours. Images were treated with ImageJ 1.42q (National Institutes of Health), and movies were assembled using the same software.

Antibodies and reagents

Antibodies to DAXX (sc-7152) and ATRX (sc-10078 for immunofluorescence, sc-15408 for immunoblotting) were from Santa Cruz Biotechnology; TRF2 (05-521) from Millipore; ASF1A (2990) and CENP-A (2186) from Cell Signaling Technology; PML (ab53773 for immunoprecipitation and immunofluorescence; ab50637 for immunoblots), H3 (ab1791), and H4 (ab10158) from Abcam; and GFP (11814460001) from Roche. Antibodies to HIRA were from Peter Adams (CR-UK Beatson Institute, Glasgow), PML (5E10) from Roel van Driel (E.C. Slater Institute, Amsterdam), and lamin B1 from Brigitte Buendia (Université Paris Diderot, Paris). Antibodies against H3.3 were from Millipore (09-838). Alexa Fluor 594 anti-goat (A-21468) was from Invitrogen. DyLight 549 anti-rabbit (711-505-152); and Cy3-, Cy2-, AMCA-, Dylight 488-, and HRP-conjugated antibodies were from Jackson Laboratories. For immunolabeling, primary antibodies were diluted 1:100 except for TRF2 (1:200), ASF1A (1:50), and CENP-A (1:400); secondary antibodies were diluted 1:200 except for Alexa Fluor 594 anti-goat (1:1000); DyLight 549 anti-rabbit (1:800) and AMCA-conjugated antibodies (1:100). For immunoblotting, antibodies were diluted as follows: GFP 1:10,000, ATRX and DAXX 1:1000, lamin B1 1:500, H3 1:5000, and HRP-conjugated 1:7000.

Immunoprecipitation and GFP-Trap pull-down

PML was immunoprecipitated from cells lysed by probe sonication (three times for 5 sec) in 20 mM Tris-HCl (pH 7.5), 150 mM NaCl, 1 mM EDTA, 1 mM EGTA, 1% Triton X-100, and a cocktail of protease inhibitors (lysis buffer). The lysate was sedimented at 10,000*g* for 15 min at 4°C, and the supernatant used for immunoprecipitation using anti-PML antibodies (10 μg for a lysate of 4 million cells), overnight at 4°C, after a pre-clearing with Protein A Dynabeads. Immune complexes were washed five times in PBS/0.1% Triton X-100 and dissolved in SDS sample buffer.

GFP-Trap pull-downs EGFP-PML (PML isoform V) were done using the magnetic GFP-Trap_M Kit as described by the manufacturer (Chromotek) except that cells were lysed in the lysis buffer described above.

Immunofluorescence

Cells were fixed with 3% paraformaldehyde for 15 min and permeabilized with 0.1% Triton X-100/0.01% Tween 20/2% BSA for 30 min. Cells were incubated with primary antibodies for 45 min, washed in PBS/0.01% Tween 20/2% BSA, and incubated with secondary antibodies for 45 min. DNA was stained with 0.1 μg/mL DAPI, and coverslips were mounted with Mowiol 4-88 (Polysciences). For in situ extraction, cells were treated on coverslips with 0.1% Triton and 1 M NaCl in PBS for 30 min at 37°C before fixation. Images from the middle plane of the nucleus were captured with a 100× objective (NA 1.4) on a CellR wide-field Imaging Station (Olympus). For deconvoluted pictures, images were captured with a 100× objective (NA 1.4) on a PersonalDV (Delta Vision) wide-field imaging station (Applied Precision), and deconvoluted with the integrated software. Images were treated with ImageJ 1.42q (National Institutes of Health). To analyze overlap between different signals, we measured fluorescence intensity profiles along a defined line using Plot Profile in ImageJ. To analyze the surface distribution of the fluorescent signal, a region corresponding to the contour of the nucleus was selected, and the fluorescence intensity of each pixel inside this area was plotted on a 3D graph using the Interactive 3D Surface Plot program in ImageJ (K.U. Barthel, Internationale Medieninformatik).

FRAP analysis

FRAP experiments were done 24 h after transfection (except for the results shown in Fig. 6, which were performed after 96 h) using a SuperApochromat 60×/1.35 oil objective and an Olympus FluoView 1000 laser scanning confocal microscope. Cells were kept at 37°C in a humid 5% CO_2 atmosphere. EGFP fluorescence was followed using a multiline Argon laser with low output power at 488 nm. Photobleaching was done with a 405-nm diode laser at maximum power, fitted to a SIM scanner for laser stimulation simultaneously to imaging. An ~2-μm diameter circle to be bleached was defined, and pictures were taken every 20 sec over 30 min. The first acquisition was made 20 sec before photobleaching to measure pre-bleach fluorescence, and the second acquisition was made during photobleaching to measure its efficiency. To analyze fluorescence recovery in the bleached area, images were treated with ImageJ. For each series, three areas were selected as follows: "bleached" (bleached area), "control" (nonbleached area in the nucleus), and "background" (background signal outside the nucleus). Mean gray values were measured in the three areas ($I_{bleached}$, $I_{control}$, and $I_{background}$, respectively) for each time point,

and the corrected fluorescence intensity of the bleached area (I) was calculated by $I = (I_{bleached} - I_{background})/(I_{control} - I_{background})$. This correction takes into account photobleaching due to illumination and the lower amount of fluorescent molecules after photobleaching. Data were normalized and converted into a percent of fluorescence intensity before bleaching (100%). Statistical analysis for indicated time points was performed using an unpaired Student's *t*-test.

Cell extraction

For preparation of total cell extracts, cells were washed in PBS and suspended in sample buffer (3000 cells per μL). For extractions, cells were washed in PBS and extracted for 15 min on ice with 1% Triton X-100 in 10 mM HEPES (pH 7.9), 10 mM KCl, 1.5 mM $MgCl_2$, 1 mM DTT, 0.1 mM PMSF, and a protease inhibitor cocktail. Lysed cells were centrifuged at 20,000*g* for 10 min at 4°C, and the pellet (insoluble fraction) was dissolved in SDS sample buffer (3000 cell-equivalent per μL). Proteins of the supernatant (soluble fraction) were precipitated with trichloroacetic acid and dissolved in SDS sample buffer at 3000 cell-equivalent per μL.

Western blotting

Samples were resolved in a 4%–20% SDS-PAGE gel and transferred to a nitrocellulose membrane, and the membrane was blocked in TBS/0.05% Tween 20 (TBST) and 5% milk for 30 min at 37°C. Membranes were incubated with primary and secondary antibodies for 45 min each at room temperature with a 3× wash in TBST in between. Horseradish peroxidase activity was detected by enhanced chemiluminescence.

Acknowledgments

We thank Peter Adams (CR-UK Beatson Institute, Glasgow) for HIRA antibodies; Roel van Driel (E.C. Slater Institute, Amsterdam) for PML antibodies; Brigitte Buendia (Université Paris Diderot, Paris) for lamin B1 antibodies; Jean-Yves Thuret (CEA Saclay) for plasmids encoding ASF1A-mCherry; David J. Picketts (The Ottawa Health Research Institute, Ottawa) for plasmid pRK5-Flag-DAXX; Harutaka Katano (National Institute of Infectious Diseases, Toyama) for the pEGFP-PML plasmid; and Maïté Coppey (Institut Jacques Monod, Paris) for the pmCherry-C vector and plasmids containing mCherry-H4 and EGFP-H4 cDNAs. We also thank Kristin Vekterud for technical assistance. This work was supported by the Norwegian Cancer Society, the Research Council of Norway, and the Norwegian Center for Stem Cell Research to P.C. E.D. was supported by Health South-East Norway.

References

Ahmad K, Henikoff S. 2002. The histone variant H3.3 marks active chromatin by replication-independent nucleosome assembly. *Mol Cell* **9:** 1191–1200.

Balaji S, Iyer LM, Aravind L. 2009. HPC2 and ubinuclein define a novel family of histone chaperones conserved throughout eukaryotes. *Mol Biosyst* **5:** 269–275.

Banumathy G, Somaiah N, Zhang R, Tang Y, Hoffmann J, Andrake M, Ceulemans H, Schultz D, Marmorstein R, Adams PD. 2009. Human UBN1 is an ortholog of yeast Hpc2p and has an essential role in the HIRA/ASF1a chromatin-remodeling pathway in senescent cells. *Mol Cell Biol* **29:** 758–770.

Boquest AC, Shahdadfar A, Fronsdal K, Sigurjonsson O, Tunheim SH, Collas P, Brinchmann JE. 2005. Isolation and transcription profiling of purified uncultured human stromal stem cells: Alteration of gene expression after in vitro cell culture. *Mol Biol Cell* **16:** 1131–1141.

Chow CM, Georgiou A, Szutorisz H, Maia e Silva A, Pombo A, Barahona I, Dargelos E, Canzonetta C, Dillon N. 2005. Variant histone H3.3 marks promoters of transcriptionally active genes during mammalian cell division. *EMBO Rep* **6:** 354–360.

Daury L, Chailleux C, Bonvallet J, Trouche D. 2006. Histone H3.3 deposition at E2F-regulated genes is linked to transcription. *EMBO Rep* **7:** 66–71.

Delbarre E, Jacobsen BM, Reiner AH, Sorensen AL, Kuntziger T, Collas P. 2010. Chromatin environment of histone variant H3.3 revealed by quantitative imaging and genome-scale chromatin and DNA immunoprecipitation. *Mol Biol Cell* **21:** 1872–1884.

Drane P, Ouararhni K, Depaux A, Shuaib M, Hamiche A. 2010. The death-associated protein DAXX is a novel histone chaperone involved in the replication-independent deposition of H3.3. *Genes Dev* **24:** 1253–1265.

Ederveen TH, Mandemaker IK, Logie C. 2011. The human histone H3 complement anno 2011. *Biochim Biophys Acta* **1809:** 577–586.

Elsasser SJ, Huang H, Lewis PW, Chin JW, Allis CD, Patel DJ. 2012. DAXX envelops an H3.3–H4 dimer for H3.3-specific recognition. *Nature* **491:** 560–565.

English CM, Maluf NK, Tripet B, Churchill ME, Tyler JK. 2005. ASF1 binds to a heterodimer of histones H3 and H4: A two-step mechanism for the assembly of the H3–H4 heterotetramer on DNA. *Biochemistry* **44:** 13673–13682.

English CM, Adkins MW, Carson JJ, Churchill ME, Tyler JK. 2006. Structural basis for the histone chaperone activity of Asf1. *Cell* **127:** 495–508.

Eustermann S, Yang JC, Law MJ, Amos R, Chapman LM, Jelinska C, Garrick D, Clynes D, Gibbons RJ, Rhodes D, et al. 2011. Combinatorial readout of histone H3 modifications specifies localization of ATRX to heterochromatin. *Nat Struct Mol Biol* **18:** 777–782.

Galvani A, Courbeyrette R, Agez M, Ochsenbein F, Mann C, Thuret JY. 2008. In vivo study of the nucleosome assembly functions of ASF1 histone chaperones in human cells. *Mol Cell Biol* **28:** 3672–3685.

Gaustad KG, Boquest AC, Anderson BE, Gerdes AM, Collas P. 2004. Differentiation of human adipose tissue stem cells using extracts of rat cardiomyocytes. *Biochem Biophys Res Commun* **314:** 420–427.

Geng Y, Monajembashi S, Shao A, Cui D, He W, Chen Z, Hemmerich P, Tang J. 2012. Contribution of the C-terminal regions of promyelocytic leukemia protein (PML) isoforms II and V to PML nuclear body formation. *J Biol Chem* **287:** 30729–30742.

Gibbons RJ, McDowell TL, Raman S, O'Rourke DM, Garrick D, Ayyub H, Higgs DR. 2000. Mutations in *ATRX*, encoding a SWI/SNF-like protein, cause diverse changes in the pattern of DNA methylation. *Nat Genet* **24:** 368–371.

Goldberg AD, Banaszynski LA, Noh KM, Lewis PW, Elsaesser SJ, Stadler S, Dewell S, Law M, Guo X, Li X, et al. 2010. Distinct factors control histone variant H3.3 localization at specific genomic regions. *Cell* **140:** 678–691.

Groth A, Ray-Gallet D, Quivy JP, Lukas J, Bartek J, Almouzni G. 2005. Human Asf1 regulates the flow of S phase histones during replicational stress. *Mol Cell* **17:** 301–311.

Groth A, Corpet A, Cook AJ, Roche D, Bartek J, Lukas J, Almouzni G. 2007. Regulation of replication fork progression through histone supply and demand. *Science* **318:** 1928–1931.

Hake SB, Allis CD. 2006. Histone H3 variants and their potential role in indexing mammalian genomes: The "H3 barcode hypothesis." *Proc Natl Acad Sci* **103:** 6428–6435.

Ishov AM, Vladimirova OV, Maul GG. 2004. Heterochromatin and ND10 are cell-cycle regulated and phosphorylation-dependent alternate nuclear sites of the transcription repressor Daxx and SWI/SNF protein ATRX. *J Cell Sci* **117:** 3807–3820.

Iwase S, Xiang B, Ghosh S, Ren T, Lewis PW, Cochrane JC, Allis CD, Picketts DJ, Patel DJ, Li H, et al. 2011. ATRX ADD domain links an atypical histone methylation recognition mechanism to human mental-retardation syndrome. *Nat Struct Mol Biol* **18:** 769–776.

Jiang WQ, Nguyen A, Cao Y, Chang AC, Reddel RR. 2011. HP1-mediated formation of alternative lengthening of telomeres-associated PML bodies requires HIRA but not ASF1a. *PLoS ONE* **6:** e17036.

Jin C, Felsenfeld G. 2006. Distribution of histone H3.3 in hematopoietic cell lineages. *Proc Natl Acad Sci* **103:** 574–579.

Jin C, Zang C, Wei G, Cui K, Peng W, Zhao K, Felsenfeld G. 2009. H3.3/H2A.Z double variant-containing nucleosomes mark 'nucleosome-free regions' of active promoters and other regulatory regions. *Nat Genet* **41:** 941–945.

Kimura H. 2005. Histone dynamics in living cells revealed by photobleaching. *DNA Repair (Amst)* **4:** 939–950.

Lewis PW, Elsaesser SJ, Noh KM, Stadler SC, Allis CD. 2010. Daxx is an H3.3-specific histone chaperone and cooperates with ATRX in replication-independent chromatin assembly at telomeres. *Proc Natl Acad Sci* **107:** 14075–14080.

Marzluff WF, Wagner EJ, Duronio RJ. 2008. Metabolism and regulation of canonical histone mRNAs: Life without a poly(A) tail. *Nat Rev Genet* **9:** 843–854.

McDowell TL, Gibbons RJ, Sutherland H, O'Rourke DM, Bickmore WA, Pombo A, Turley H, Gatter K, Picketts DJ, Buckle VJ, et al. 1999. Localization of a putative transcriptional regulator (ATRX) at

pericentromeric heterochromatin and the short arms of acrocentric chromosomes. *Proc Natl Acad Sci* **96:** 13983–13988.
McKittrick E, Gafken PR, Ahmad K, Henikoff S. 2004. Histone H3.3 is enriched in covalent modifications associated with active chromatin. *Proc Natl Acad Sci* **101:** 1525–1530.
Mello JA, Sillje HH, Roche DM, Kirschner DB, Nigg EA, Almouzni G. 2002. Human Asf1 and CAF-1 interact and synergize in a repair-coupled nucleosome assembly pathway. *EMBO Rep* **3:** 329–334.
Michod D, Bartesaghi S, Khelifi A, Bellodi C, Berliocchi L, Nicotera P, Salomoni P. 2012. Calcium-dependent dephosphorylation of the histone chaperone DAXX regulates H3.3 loading and transcription upon neuronal activation. *Neuron* **74:** 122–135.
Mito Y, Henikoff JG, Henikoff S. 2005. Genome-scale profiling of histone H3.3 replacement patterns. *Nat Genet* **37:** 1090–1097.
Natsume R, Eitoku M, Akai Y, Sano N, Horikoshi M, Senda T. 2007. Structure and function of the histone chaperone CIA/ASF1 complexed with histones H3 and H4. *Nature* **446:** 338–341.
Newhart A, Rafalska-Metcalf IU, Yang T, Negorev DG, Janicki SM. 2012. Single cell analysis of Daxx and ATRX-dependent transcriptional repression. *J Cell Sci* doi: 10.1242/jcs.110148.
Rai TS, Puri A, McBryan T, Hoffman J, Tang Y, Pchelintsev NA, van Tuyn J, Marmorstein R, Schultz DC, Adams PD. 2011. Human CABIN1 is a functional member of the human HIRA/UBN1/ASF1a histone H3.3 chaperone complex. *Mol Cell Biol* **31:** 4107–4118.
Ramachandran S, Vogel L, Strahl BD, Dokholyan NV. 2011. Thermodynamic stability of histone H3 is a necessary but not sufficient driving force for its evolutionary conservation. *PLoS Comput Biol* **7:** e1001042.
Ray-Gallet D, Quivy JP, Scamps C, Martini EM, Lipinski M, Almouzni G. 2002. HIRA is critical for a nucleosome assembly pathway independent of DNA synthesis. *Mol Cell* **9:** 1091–1100.
Ray-Gallet D, Woolfe A, Vassias I, Pellentz C, Lacoste N, Puri A, Schultz DC, Pchelintsev NA, Adams PD, Jansen LE, et al. 2011. Dynamics of histone H3 deposition in vivo reveal a nucleosome gap-filling mechanism for H3.3 to maintain chromatin integrity. *Mol Cell* **44:** 928–941.
Schwartzentruber J, Korshunov A, Liu XY, Jones DT, Pfaff E, Jacob K, Sturm D, Fontebasso AM, Quang DA, Tonjes M, et al. 2012. Driver mutations in histone H3.3 and chromatin remodelling genes in paediatric glioblastoma. *Nature* **482:** 226–231.
Shi L, Wang J, Hong F, Spector DL, Fang Y. 2011. Four amino acids guide the assembly or disassembly of *Arabidopsis* histone H3.3-containing nucleosomes. *Proc Natl Acad Sci* **108:** 10574–10578.
Smith S, Stillman B. 1989. Purification and characterization of CAF-I, a human cell factor required for chromatin assembly during DNA replication in vitro. *Cell* **58:** 15–25.
Stuurman N, de Graaf A, Floore A, Josso A, Humbel B, de Jong L, van Driel R. 1992. A monoclonal antibody recognizing nuclear matrix-associated nuclear bodies. *J Cell Sci* **101:** 773–784.
Sutcliffe EL, Parish IA, He YQ, Juelich T, Tierney ML, Rangasamy D, Milburn PJ, Parish CR, Tremethick DJ, Rao S. 2009. Dynamic histone variant exchange accompanies gene induction in T cells. *Mol Cell Biol* **29:** 1972–1986.
Szenker E, Ray-Gallet D, Almouzni G. 2011. The double face of the histone variant H3.3. *Cell Res* **21:** 421–434.
Tagami H, Ray-Gallet D, Almouzni G, Nakatani Y. 2004. Histone H3.1 and H3.3 complexes mediate nucleosome assembly pathways dependent or independent of DNA synthesis. *Cell* **116:** 51–61.
Talbert PB, Henikoff S. 2010. Histone variants—ancient wrap artists of the epigenome. *Nat Rev Mol Cell Biol* **11:** 264–275.
Tamura T, Smith M, Kanno T, Dasenbrock H, Nishiyama A, Ozato K. 2009. Inducible deposition of the histone variant H3.3 in interferon-stimulated genes. *J Biol Chem* **284:** 12217–12225.
Tang J, Wu S, Liu H, Stratt R, Barak OG, Shiekhattar R, Picketts DJ, Yang X. 2004. A novel transcription regulatory complex containing death domain-associated protein and the ATR-X syndrome protein. *J Biol Chem* **279:** 20369–20377.
Tang Y, Poustovoitov MV, Zhao K, Garfinkel M, Canutescu A, Dunbrack R, Adams PD, Marmorstein R. 2006. Structure of a human ASF1a–HIRA complex and insights into specificity of histone chaperone complex assembly. *Nat Struct Mol Biol* **13:** 921–929.
Tang Y, Puri A, Ricketts MD, Rai TS, Hoffmann J, Hoi E, Adams PD, Schultz DC, Marmorstein R. 2012. Identification of an Ubinuclein 1 region required for stability and function of the human HIRA/UBN1/CABIN1/ASF1a histone H3.3 chaperone complex. *Biochemistry* **51:** 2366–2377.
Tyler JK, Collins KA, Prasad-Sinha J, Amiott E, Bulger M, Harte PJ, Kobayashi R, Kadonaga JT. 2001. Interaction between the *Drosophila* CAF-1 and ASF1 chromatin assembly factors. *Mol Cell Biol* **21:** 6574–6584.
Weidtkamp-Peters S, Lenser T, Negorev D, Gerstner N, Hofmann TG, Schwanitz G, Hoischen C, Maul G, Dittrich P, Hemmerich P. 2008. Dynamics of component exchange at PML nuclear bodies. *J Cell Sci* **121:** 2731–2743.
Wong LH, Ren H, Williams E, McGhie J, Ahn S, Sim M, Tam A, Earle E, Anderson MA, Mann J, et al. 2009. Histone H3.3 incorporation provides a unique and functionally essential telomeric chromatin in embryonic stem cells. *Genome Res* **19:** 404–414.
Wong LH, McGhie JD, Sim M, Anderson MA, Ahn S, Hannan RD, George AJ, Morgan KA, Mann JR, Choo KH. 2010. ATRX interacts with H3.3 in maintaining telomere structural integrity in pluripotent embryonic stem cells. *Genome Res* **20:** 351–360.
Wu G, Broniscer A, McEachron TA, Lu C, Paugh BS, Becksfort J, Qu C, Ding L, Huether R, Parker M, et al. 2012. Somatic histone H3 alterations in pediatric diffuse intrinsic pontine gliomas and non-brainstem glioblastomas. *Nat Genet* **44:** 251–253.
Xue Y, Gibbons R, Yan Z, Yang D, McDowell TL, Sechi S, Qin J, Zhou S, Higgs D, Wang W. 2003. The ATRX syndrome protein forms a chromatin-remodeling complex with Daxx and localizes in promyelocytic leukemia nuclear bodies. *Proc Natl Acad Sci* **100:** 10635–10640.
Zhang R, Poustovoitov MV, Ye X, Santos HA, Chen W, Daganzo SM, Erzberger JP, Serebriiskii IG, Canutescu AA, Dunbrack RL, et al. 2005. Formation of MacroH2A-containing senescence-associated heterochromatin foci and senescence driven by ASF1a and HIRA. *Dev Cell* **8:** 19–30.

Received May 3, 2012; accepted in revised form November 30, 2012.